



Title	Carbohydrates as Hard Segments for Sustainable Elastomers: Carbohydrates Direct the Self-Assembly and Mechanical Properties of Fully Bio-Based Block Copolymers
Author(s)	Isono, Takuya; Nakahira, Saki; Hsieh, Hui-Ching; Katsuhara, Satoshi; Mamiya, Hiroaki; Yamamoto, Takuya; Chen, Wen-Chang; Borsali, Redouane; Tajima, Kenji; Satoh, Toshifumi
Citation	Macromolecules, 53(13), 5408-5417 https://doi.org/10.1021/acs.macromol.0c00611
Issue Date	2020-07-14
Doc URL	http://hdl.handle.net/2115/82217
Rights	This document is the Accepted Manuscript version of a Published Work that appeared in final form in Macromolecules, copyright © American Chemical Society after peer review and technical editing by the publisher. To access the final edited and published work see https://pubs.acs.org/doi/10.1021/acs.macromol.0c00611
Type	article (author version)
File Information	main_text - rev2 (final).pdf



[Instructions for use](#)

Carbohydrates as Hard Segments for Sustainable Elastomers: Carbohydrates Direct the Self-assembly and Mechanical Properties of Fully Bio-based Block Copolymers

Takuya Isono,^{,†} Saki Nakahira,[‡] Hui-Ching Hsieh,[¶] Satoshi Katsuhara,[‡] Hiroaki Mamiya,[¶]
Takuya Yamamoto,[†] Wen-Chang Chen,[¶] Redouane Borsali,[§] Kenji Tajima,[†] Toshifumi Satoh^{*,†}*

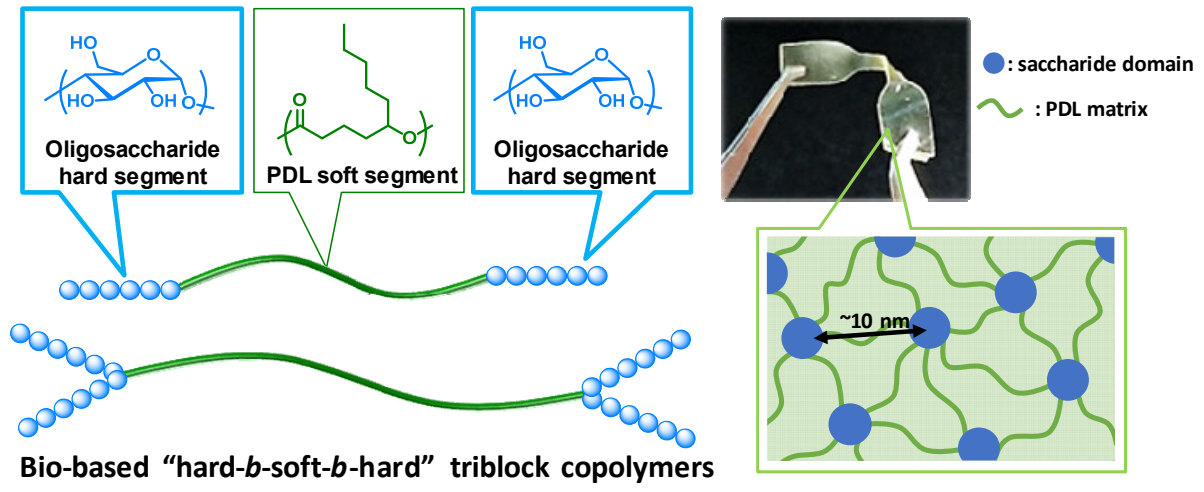
[†]Faculty of Engineering; [‡]Graduate School of Chemical Sciences and Engineering, Hokkaido University, Sapporo 060-8628, Japan.

[¶]Department of Chemical Engineering, National Taiwan University, Taipei 10617, Taiwan.

[¶]National Institute for Materials Science, Tsukuba 305-0047, Japan.

[§]Univ. Grenoble Alps, CNRS, CERMAV, Grenoble 38000, France.

TOC Graphic



Abstract

A series of fully bio-based block copolymers (BCPs) consisting of maltooligosaccharides (maltose, maltotriose, maltotetraose, and maltohexaose; A block) and poly(δ -decanolactone) (PDL; B block), with ABA-, A₂BA₂-, A₃BA₃-, A(BA)₂-, and A₂(BA)₂-type architectures, were synthesized to demonstrate the potential of oligosaccharides as novel hard segments for bio-based elastomers. To understand the correlation between the BCP molecular structure and material properties, the BCPs were designed to have comparable molecular weights (ca. 12k) and total numbers of glucose units (12). Morphological analysis revealed the formation of body-centered cubic sphere and hexagonally close-packed cylinder (HEX) morphologies depending on the branched architecture (interdomain distance 9.7–14.4 nm). While the PDL homopolymer is a viscous liquid due to its low T_g and amorphous nature, all BCPs exhibited elastomeric properties, confirming that the oligosaccharide blocks segregated to form the hard domains to crosslink the rubbery PDL chains. Tensile testing revealed that the mechanical properties of the BCPs were mainly determined by the microphase-separated structure and less affected by the length of each oligosaccharide chain. The HEX-forming A₂BA₂- and A₃BA₃-type BCPs exhibited Young's moduli of ~6 MPa, which is comparable to well-known styrene-based thermoplastic elastomers. Furthermore, a readily available polydisperse maltooligosaccharide was employed to synthesize an A₂BA₂-type BCP with a higher molecular weight PDL block (20k), which exhibited a Young's modulus of ~6 MPa and an elongation at break of ~700%. These results demonstrate that oligosaccharides are a sustainable alternative to the petroleum-derived synthetic hard segments (e.g., polystyrene), thereby opening up a new avenue for fully bio-based soft material design.

Introduction

Carbohydrates, including monosaccharides, oligosaccharides, and polysaccharides, have recently attracted growing attention as the key renewable resources produced by plants from carbon dioxide.¹⁻⁵ Owing to their renewable nature, carbohydrates are now recognized as suitable starting materials for the production of environmentally benign polymeric materials.⁵⁻⁹ Indeed, some of commercially available polymers, such as poly(lactic acid), poly(butylene succinate), poly(hydroxylalkanoate), and poly(ethylene furanoate), are produced (partly) from monomers of carbohydrate origin.⁵ However, to synthesize such polymers from the naturally occurring carbohydrates, several chemical and/or biological processes are required, during which the unique characteristics of the carbohydrates, such as their biocompatibility, biodegradability, biological activity, and self-assembling ability, are completely lost. Therefore, it is of particular interest to utilize the carbohydrates in straightforward manner to create high value-added polymers without losing their unique and original characteristics.

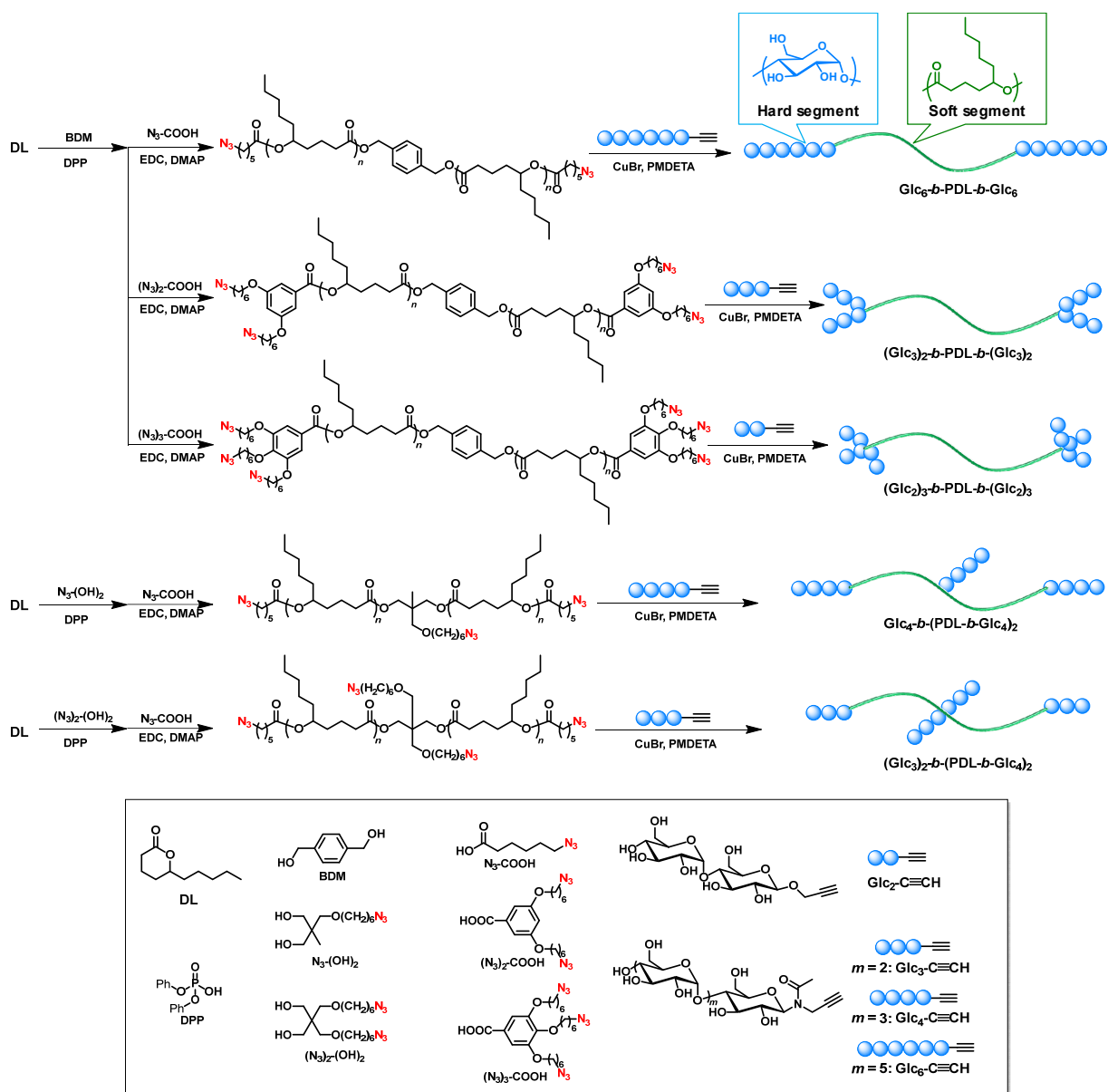
Polysaccharides, such as cellulose, amylose, and their derivatives, have long been utilized as thermoplastics and fibers while retaining their major unique characteristics. Despite the long history of utilizing polysaccharides in commodity polymers, their range of applications has been limited due to their intrinsically hard and rigid properties. Thus, the exploration of carbohydrate-based elastomeric materials is of fundamental interest, in particular in the context of their use in various commodity and fine applications.

To impart soft and elastic properties to carbohydrates, the hybridization of a hard and rigid carbohydrate segment with a rubbery polymer chain is essential. In addition, a “hard-*b*-soft-*b*-hard” type triblock architecture as well as a microphase separation between the soft and hard

blocks are also important to achieve elastomeric properties, such as in the cases of the well-known polystyrene-*b*-polyisoprene-*b*-polystyrene and polystyrene-*b*-polybutadiene-*b*-polystyrene thermoplastic elastomers.^{10,11} It should be noted here that previous studies by our group and Sita's group revealed that block copolymers (BCPs) consisting of hydrophobic polymers and oligosaccharides readily self-assembled into microphase-separated structures due to the strong segregation between the blocks, which was further enhanced by the rigid rod nature of the oligosaccharide.¹²⁻²³ We therefore envisioned that the integration of a rubbery hydrophobic polymer at the middle block and oligo/polysaccharide hard segments at the outer blocks could provide a novel bio-based elastomer, in which the microphase-separated carbohydrate hard domains act as a physical crosslink for the rubbery chains.

Thus, we herein demonstrate the potential of oligosaccharides as the hard segment of bio-based elastomers through the synthesis and characterization of fully bio-based "hard-*b*-soft-*b*-hard" triblock copolymers consisting of maltooligosaccharides as the hard segments and poly(δ -decanolactone) (PDL) as the soft segment. Due to the amorphous nature, relatively high glass transition temperature (T_g), good solubility in polar organic solvents, and commercial availability of structurally well-defined samples, low molecular weight amylose (i.e., maltooligosaccharides) should be the best choice as the hard segment for a model study. Meanwhile, PDL is an amorphous aliphatic polyester with a low T_g (approx. -60 °C),²⁴ which can be readily obtained by the ring-opening polymerization (ROP) of the biologically-available δ -decanolactone (DL).²⁵ Since the microphase-separated structure is one of the dominant factors in affecting the mechanical properties,^{26,27} it is also of fundamental interest to evaluate the elastomer performances using a series of oligosaccharide-containing BCPs with varied morphologies while fixing the other molecular parameters. According to our previous studies, control over the

microphase-separated morphology can be achieved by incorporating a branched architecture without changing the molecular weight and volume fraction of the BCPs.^{13,14} Thus, we designed and synthesized a series of fully bio-based BCPs consisting of maltooligosaccharide (A block; maltose (Glc₂), maltotriose (Glc₃), maltotetraose (Glc₄), and maltohexaose (Glc₆)) and PDL (B block) with ABA-, A₂BA₂-, A₃BA₃-, A(BA)₂-, and A₂(BA)₂-type architectures as the model system. For the systematic study into the correlation between the morphology and the mechanical properties, the total molecular weight of the PDL segment and total number of glucose units in the BCPs were fixed at ca. 12k and 12, respectively. BCP synthesis is carried out in three steps involving the ROP of DL, end-functionalization, and a click reaction with an ethynyl-functionalized oligosaccharide, as outlined in Scheme 1. In addition, an extensive study into the relationship between the BCP architecture/morphology and the mechanical properties is carried out. Overall, we wish to demonstrate that oligo/polysaccharides can be good candidates as the bio-based hard segments of sustainable elastomers. Although bio-based polymers, such as polylactide,²⁸⁻³² poly(γ -methyl- α -methylene- γ -butyrolactone),³³ rosin-based polymers,³⁴ and poly(itaconimide)³⁵ have been reported as the hard segments of fully bio-based elastomers, our study could represent the first example of using oligo/polysaccharides in designing such materials.



Scheme 1. Syntheses of $\text{Glc}_6\text{-}b\text{-PDL-}b\text{-Glc}_6$, $(\text{Glc}_3)_2\text{-}b\text{-PDL-}b\text{-(Glc}_3)_2$, $(\text{Glc}_2)_3\text{-}b\text{-PDL-}b\text{-(Glc}_2)_3$, $\text{Glc}_4\text{-}b\text{-(PDL-}b\text{-Glc}_4)_2$, and $(\text{Glc}_3)_2\text{-}b\text{-(PDL-}b\text{-Glc}_3)_2$.

Results and Discussion

Synthesis

For preparation of the ABA-, A₂BA₂-, and A₃BA₃-type BCPs (Scheme 1), the synthesis began from the diphenyl phosphate (DPP)-catalyzed solvent-free ROP of DL using 1,4-benzenedimethanol (BDM) as the initiator,^{18,36,37} yielding a PDL diol (HO-PDL-OH) with an absolute number-average molecular weight ($M_{n,NMR}$) of 11300 g mol⁻¹ and a narrow dispersity (D) of 1.11. The chain end hydroxyl groups were then reacted with 6-azidohexanoic acid (N₃-COOH) in the presence of EDC and DMAP to produce an α,ω -diazido-functionalized PDL (N₃-PDL-N₃) with an $M_{n,NMR}$ and a D of 10900 g mol⁻¹ and 1.10, respectively. The successful introduction of the azido group was confirmed by ¹H NMR spectroscopy (Figure S1). In a similar manner, the $\alpha,\alpha,\omega,\omega$ -tetraazido-functionalized PDL ((N₃)₂-PDL-(N₃)₂; $M_{n,NMR}$ = 11100 g mol⁻¹, D = 1.11) and the $\alpha,\alpha,\alpha,\omega,\omega,\omega$ -hexaazido-functionalized PDL ((N₃)₃-PDL-(N₃)₃; $M_{n,NMR}$ = 13600 g mol⁻¹, D = 1.06) were prepared by treating HO-PDL-OH with 3,5-bis(6-azidohexyloxy)benzoic acid ((N₃)₂-COOH) and 3,4,5-tris(6-azidohexyloxy)benzoic acid ((N₃)₃-COOH), respectively (see Figures S2 and S3 for the ¹H NMR spectra). For preparation of the A(AB)₂- and A₂(AB)₂-type BCPs (Scheme 1), an in-chain azido-functionalized PDL diol (N₃-(PDL-OH)₂; $M_{n,NMR}$ = 12500 g mol⁻¹, D = 1.12) and an in-chain diazido-functionalized PDL diol ((N₃)₂-(PDL-OH)₂; $M_{n,NMR}$ = 13100 g mol⁻¹, D = 1.13) were prepared by the DPP-catalyzed ROPs of DL using 2-[(6-azidohexyloxy)methyl]-2-methylpropane-1,3-diol (N₃-(OH)₂)¹³ and 2,2-bis((6-azidohexyloxy)methyl)propane-1,3-diol ((N₃)₂-(OH)₂)³⁸ as the initiators, respectively. Subsequently, N₃-(PDL-OH)₂ and (N₃)₂-(PDL-OH)₂ were treated with N₃-COOH to attach an azido group at each end, giving the desired triazido-functionalized PDL, i.e., N₃-(PDL-N₃)₂

($M_{n,NMR} = 11200 \text{ g mol}^{-1}$, $D = 1.12$), and the tetraazido-functionalized PDL, i.e., $(N_3)_2\text{-(PDL-N}_3)_2$ ($M_{n,NMR} = 12200 \text{ g mol}^{-1}$, $D = 1.12$), respectively (see Figures S4 and S5 for $^1\text{H NMR}$).

To synthesize the targeted BCPs containing a total of 12 glucose units, $\text{Glc}_6\text{-C}\equiv\text{CH}$, $\text{Glc}_4\text{-C}\equiv\text{CH}$, $\text{Glc}_3\text{-C}\equiv\text{CH}$, and $\text{Glc}_2\text{-C}\equiv\text{CH}$ were coupled with the diazido- ($N_3\text{-PDL-N}_3$), triazido- ($N_3\text{-(PDL-N}_3)_2$), tetraazido- ($(N_3)_2\text{-PDL-(N}_3)_2$ and $(N_3)_2\text{-(PDL-N}_3)_2$), and hexaazido-functionalized PDLs ($(N_3)_3\text{-PDL-(N}_3)_3$), respectively, under typical copper-catalyzed azido-alkyne click reaction conditions. The click reactions were performed in DMF at $60 \text{ }^\circ\text{C}$ in the presence of CuBr and PMDETA, in which a slight excess of alkyne-functionalized oligosaccharide was added with respect to the azido group. After confirming the complete consumption of the azido group by FT-IR analysis (Figures S6–S10), the reaction mixtures were subjected to treatment with a cation exchange resin followed by reprecipitation in methanol, producing white elastic materials in 49–70% yields. The successful synthesis was verified by size-exclusion chromatography (SEC), FT-IR spectroscopy, and $^1\text{H NMR}$ spectroscopy. For each product, a clear shift of the SEC elution peak toward the high-molecular-weight side was observed when compared with the corresponding azido-functionalized precursor (Figure 1). In the FT-IR spectra of the obtained BCPs, the characteristic absorption band at approximately 2100 cm^{-1} was no longer observed, confirming the quantitative consumption of the azido group by the click reaction (Figures S6–S10). In addition, $^1\text{H NMR}$ signals attributable to both the oligosaccharide and PDL segments were observed in all $^1\text{H NMR}$ spectra, along with minor signals corresponding to the end group structures, which were reasonably assignable to the expected BCP chemical structures (Figures S11–S15). These results confirmed the successful synthesis of a series of BCPs with defined structures. Based on the $^1\text{H NMR}$ analysis, the $M_{n,NMR}$ and oligosaccharide volume fraction (f_{sac}) were calculated, as summarized in Table 1.

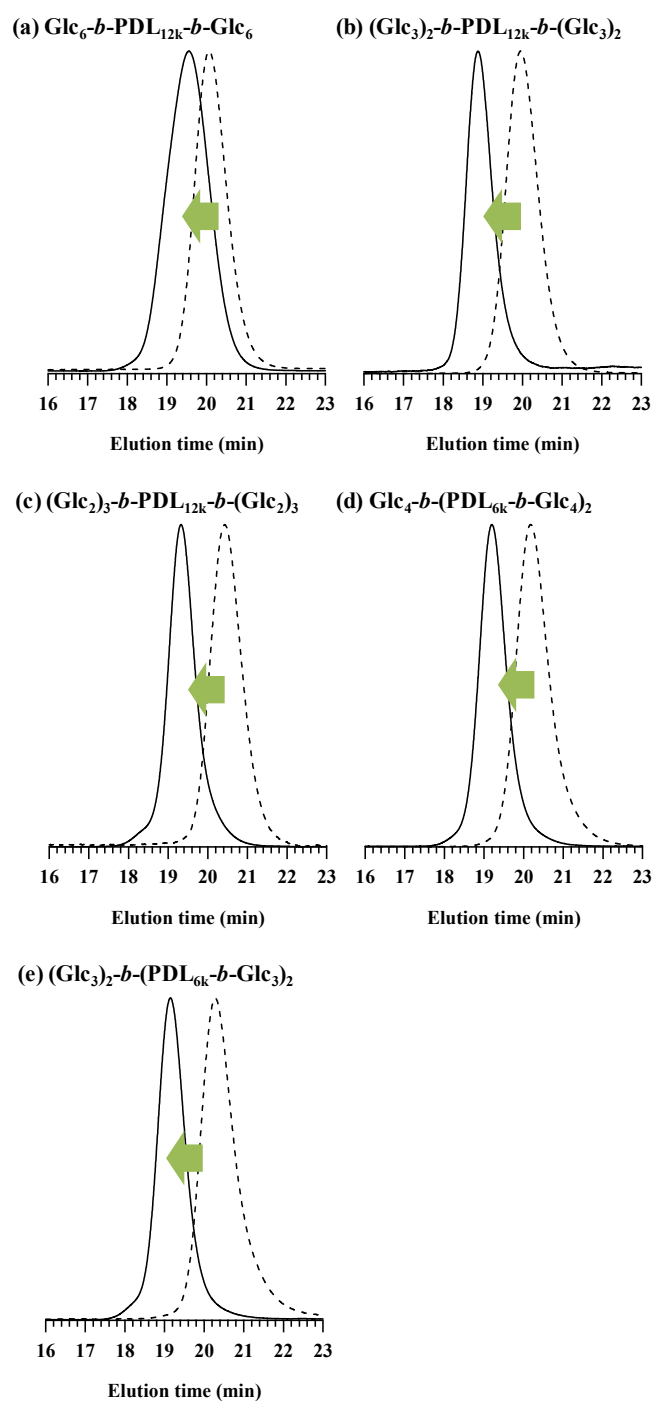


Figure 1. SEC traces of (a) $\text{Glc}_6\text{-}b\text{-PDL}\text{-}b\text{-Glc}_6$, (b) $(\text{Glc}_3)_2\text{-}b\text{-PDL}\text{-}b\text{-(Glc}_3)_2$, (c) $(\text{Glc}_2)_3\text{-}b\text{-PDL}\text{-}b\text{-(Glc}_2)_3$, (d) $\text{Glc}_4\text{-}b\text{-(PDL}\text{-}b\text{-Glc}_4)_2$, and (e) $(\text{Glc}_3)_2\text{-}b\text{-(PDL}\text{-}b\text{-Glc}_3)_2$ (eluent, DMF containing 0.01 M LiCl; flow rate, 0.60 mL min^{-1}). The solid and broken curves represent the BCP and its azido-functionalized precursor, respectively.

Table 1. Molecular characteristics of the synthesized BCPs and their corresponding azido-functionalized precursors

	azido-functionalized precursor			BCP			
	$M_{n,NMR}^a$ (g mol ⁻¹)	$M_{n,SEC}^b$ (g mol ⁻¹)	D^b	M_n^c (g mol ⁻¹)	$M_{n,SEC}^b$ (g mol ⁻¹)	D^b	f_{sac}^d
Glc ₆ - <i>b</i> -PDL- <i>b</i> -Glc ₆	10900	12100	1.10	13400	18700	1.19	0.12
(Glc ₃) ₂ - <i>b</i> -PDL- <i>b</i> -(Glc ₃) ₂	11100	13000	1.11	15300	29000	1.07	0.13
(Glc ₂) ₃ - <i>b</i> -PDL- <i>b</i> -(Glc ₂) ₃	13600	13200	1.06	15400	29000	1.11	0.11
Glc ₄ -(PDL- <i>b</i> -Glc ₄) ₂	11200	13400	1.12	16200	29500	1.12	0.12
(Glc ₃) ₂ -(PDL- <i>b</i> -Glc ₃) ₂	12200	12300	1.12	16000	30800	1.13	0.12

^aDetermined by ¹H NMR measurements in CDCl₃. ^bDetermined by SEC in DMF (containing 0.01 M LiCl) based on polystyrene calibration. ^cCalculated by: ($M_{n,NMR}$ of azido-functionalized precursor) + $m \times$ (M.W. of Glc_{*n*}-C≡CH), where the m is the number of the oligosaccharide units. ^dCalculated based on the known density value for each block: 1.36 g cm⁻³ for the oligosaccharide block and 0.97 g cm⁻³ for the PDL block.

Thermal Properties

The thermal properties of the BCPs were then tested by thermogravimetry and differential scanning calorimetry analyses (TGA and DSC, respectively) under a nitrogen atmosphere. From the TGA results, it was apparent that all BCPs were thermally stable up to ca. 240 °C, and the 5% weight loss temperature ($T_{d5\%}$) was in the range of 275–299 °C (Figure S16 and Table S1). The DSC trace of the BCPs exhibited two baseline shifts corresponding to the glass transition temperatures (T_{gs}) of the PDL ($T_{g,PDL} = -50$ to -48 °C) and the oligosaccharide blocks ($T_{g,sac} = 84$ to 143 °C) as shown in Figure 2. Remarkably, it was found that the $T_{g,sac}$ was dependent on the oligosaccharide chain length, whereby an increase in the oligosaccharide chain length

increased the $T_{g,sac}$ of the BCP. This trend is in good agreement with the reported T_g values for the unmodified maltooligosaccharides.³⁹ In contrast, the $T_{g,PDL}$ was unaffected by both the oligosaccharide chain length and the branched architecture. Importantly, no crystallization or melting peaks were observed in the DSC traces, demonstrating the amorphous nature of the BCPs. The DSC data therefore confirms that the PDL and oligosaccharide blocks in the BCPs are in the rubbery and glassy states, respectively, at room temperature, thereby rendering them suitable for elastomer applications. The service temperature of the carbohydrate-based elastomers should therefore be between $T_{g,PDL}$ and $T_{g,sac}$.

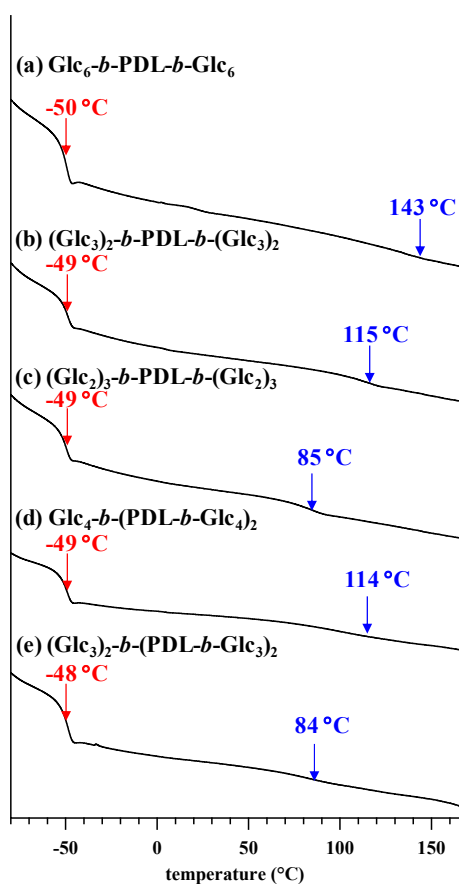


Figure 2. DSC thermograms of (a) $Glc_6-b-PDL-b-Glc_6$, (b) $(Glc_3)_2-b-PDL-b-(Glc_3)_2$, (c) $(Glc_2)_3-b-PDL-b-(Glc_2)_3$, (d) $Glc_4-b-(PDL-b-Glc_4)_2$, and (e) $(Glc_3)_2-b-(PDL-b-Glc_3)_2$ during the second heating run (under nitrogen atmosphere; heating rate, $10\text{ }^\circ\text{C min}^{-1}$).

Morphological Analysis and the Structure-Morphology Relationship

Phase separation between the PDL and oligosaccharide segments is an essential requirement to produce elastomeric properties. Thus, the above-synthesized BCPs were subjected to small-angle X-ray scattering (SAXS) and atomic force microscope (AFM) analyses to investigate the microphase-separated structure and to discuss the relationship between the BCP architecture and the morphology. For the SAXS experiments, solvent-cast films were prepared by slow evaporation from the DMF solution (33 wt%) at 60 °C for 24 h followed by vacuum drying at 60 °C for 24 h. Thermal annealing at 180 °C for 3 h was then applied to further facilitate the structural development. For the AFM experiments, nanoscale thin film samples were prepared by spin-coating the DMF solution onto a hydrophilic surface of silicon wafer followed by thermal annealing at 180 °C for 3 h.

Figure 3 summarizes the SAXS profiles of the solvent-cast BCP specimens (free-standing ca. 0.2 mm-thick films) after thermal annealing. Importantly, all BCPs exhibited an intense principle scattering (q^*) along with multiple higher ordered scattering peaks, which is an indication of microphase separation between the PDL and oligosaccharide segments. The strong hydrophilicity and conformation rigidity of the maltooligosaccharide segments render them highly incompatible to the hydrophobic PDL, which enables the microphase separation in spite of the small f_{sac} and the relatively low molecular weights.¹²⁻²³ Specifically, the SAXS profiles of $\text{Glc}_6\text{-}b\text{-PDL-}b\text{-Glc}_6$ after the thermal annealing revealed the formation of the body-centered cubic sphere (BCC) morphology, as evidenced by the characteristic scattering pattern of $q/q^* = 1, \sqrt{2}, \sqrt{3}, 2,$ and so on (Figure 3a). The inter-sphere distance ($d_{\text{s-s}}$) value of the BCC structures was calculated to be 13.6 nm based on the Bragg equation ($d_{\text{s-s}} = (2\pi/q^*) (3/2)^{1/2}$). As shown in Figure 4a, the AFM phase image of the thermally-annealed thin film on a silicon wafer clearly showed

spherical dots on the surface. This can be attributed to the spherical BCC morphology, and so is consistent with the SAXS result in the bulk state. The inter-sphere distance (d_{AFM}) was determined to be 11.9 nm by analyzing the fast Fourier transform (FFT) image, which corresponded with that determined from the SAXS result.

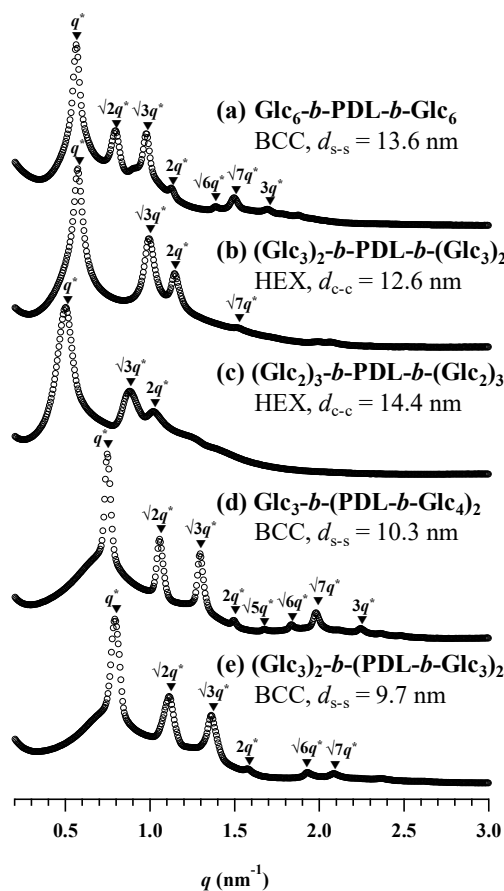


Figure 3. SAXS profiles of the solvent-casted (a) $\text{Glc}_6\text{-}b\text{-PDL-}b\text{-Glc}_6$, (b) $(\text{Glc}_3)_2\text{-}b\text{-PDL-}b\text{-}(\text{Glc}_3)_2$, (c) $(\text{Glc}_2)_3\text{-}b\text{-PDL-}b\text{-}(\text{Glc}_2)_3$, (d) $\text{Glc}_4\text{-}(\text{PDL-}b\text{-Glc}_4)_2$, and (e) $(\text{Glc}_3)_2\text{-}(\text{PDL-}b\text{-Glc}_3)_2$ specimens after thermal annealing (180 °C for 3 h).

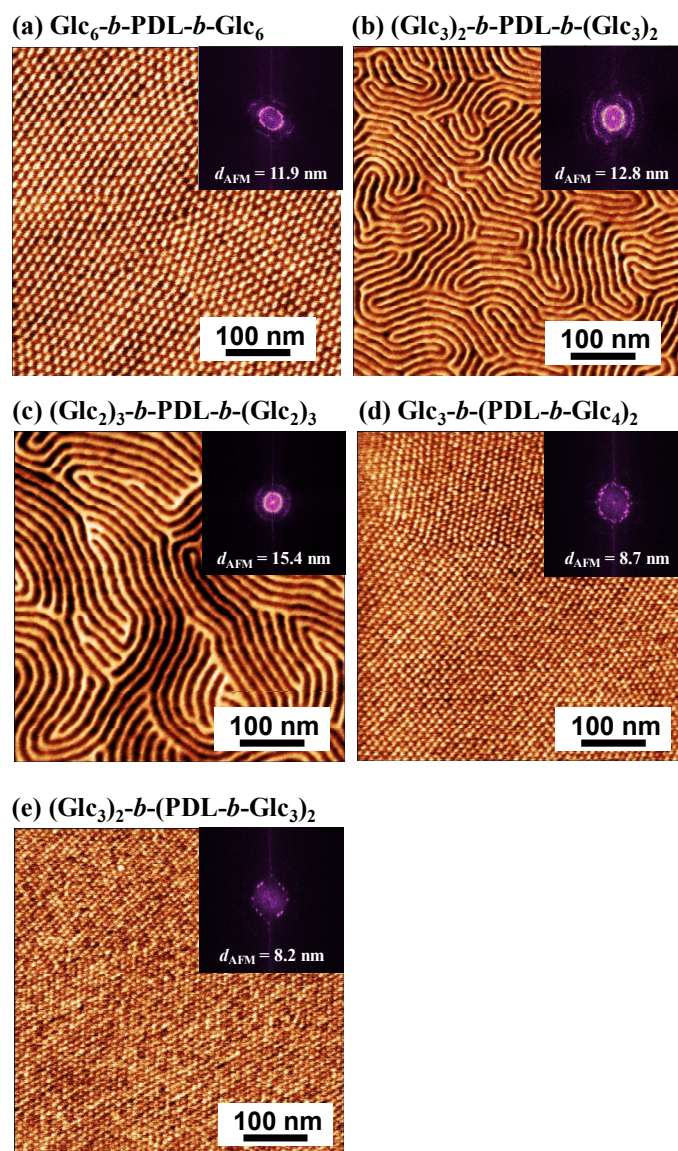


Figure 4. AFM phase images of (a) $\text{Glc}_6\text{-}b\text{-PDL-}b\text{-Glc}_6$, (b) $(\text{Glc}_3)_2\text{-}b\text{-PDL-}b\text{-}(\text{Glc}_3)_2$, (c) $(\text{Glc}_2)_3\text{-}b\text{-PDL-}b\text{-}(\text{Glc}_2)_3$, (d) $\text{Glc}_3\text{-}b\text{-}(\text{PDL-}b\text{-Glc}_4)_2$, and (e) $(\text{Glc}_3)_2\text{-}b\text{-}(\text{PDL-}b\text{-Glc}_3)_2$ thin films on a silicon wafer after thermal annealing ($180\text{ }^\circ\text{C}$ for 3 h). The insets show the corresponding FFT profiles.

Upon branching the maltohexaose segment into two maltotriose or three maltose segments, i.e., $(\text{Glc}_3)_2\text{-}b\text{-PDL-}b\text{-}(\text{Glc}_3)_2$ and $(\text{Glc}_2)_3\text{-}b\text{-PDL-}b\text{-}(\text{Glc}_2)_3$, a drastic change in the morphology was observed compared to the linear counterpart, i.e., $(\text{Glc}_3)_2\text{-}b\text{-PDL-}b\text{-}(\text{Glc}_3)_2$ and $(\text{Glc}_2)_3\text{-}b\text{-PDL-}b\text{-}$

(Glc₂)₃ exhibited the hexagonally close-packed cylinder (HEX) morphology while Glc₆-*b*-PDL-*b*-Glc₆ formed the BCC structure. In the SAXS profiles of the thermally-annealed (Glc₃)₂-*b*-PDL-*b*-(Glc₃)₂ and (Glc₂)₃-*b*-PDL-*b*-(Glc₂)₃, the scattering peak pattern of $q/q^* = 1, \sqrt{3}, 2$, and so on, was clearly observed (Figures 3b and 3c), which is typical for the HEX morphology. The HEX morphology was further confirmed by AFM observations, whereby fingerprint-like morphologies were observed in the phase images, which are typical for the horizontally-orientated HEX (Figures 4b and 4c). The difference in the morphology between the linear and branched BCPs can be explained by chain crowding at the microdomain/matrix interface.⁴⁰⁻⁴² In the case of Glc₆-*b*-PDL-*b*-Glc₆, the PDL-rich asymmetric composition gave rise to a strong driving force to bend the interface toward the minority maltohexaose domain, which resulted in the formation of the highly curved BCC morphology. In contrast, branching of the oligosaccharide segment into two or three arms increased the local chain crowding at the saccharide side of the interface, which created a driving force to produce a flat interface, leading to the less curved morphology of HEX. It is notable that the inter-cylinder distance ($d_{c-c} = (2\pi/q^*) (4/3)^{1/2}$) for (Glc₂)₃-*b*-PDL-*b*-(Glc₂)₃ ($d_{c-c} = 14.4$ nm) is apparently larger than that of (Glc₃)₂-*b*-PDL-*b*-(Glc₃)₂ ($d_{c-c} = 12.6$ nm). This could stem from the PDL chain stretching. Upon comparing (Glc₃)₂-*b*-PDL-*b*-(Glc₃)₂ and (Glc₂)₃-*b*-PDL-*b*-(Glc₂)₃, the later should have a significantly less curved interface than the former according to the degree of saccharide chain crowding at the interface. In the less curved interface, (Glc₂)₃-*b*-PDL-*b*-(Glc₂)₃ molecules are required to be packed more tightly, which forces stretching of the PDL chain, resulting in a larger domain-spacing.

Subsequently, we turned our attention to the microphase-separated structures of the BCPs possessing oligosaccharide segments at both the chain center and the chain ends, i.e., Glc₄-(PDL-

b -Glc₄)₂ and (Glc₃)₂-(PDL- b -Glc₃)₂. The thermally-annealed specimens of those BCPs exhibited a $q/q^* = 1, \sqrt{2}, \sqrt{3}, 2$ scattering pattern in their SAXS profiles (Figures 3d and 3e), confirming formation of the BCC morphology. Given that these two BCPs have a comparable volume fraction to Glc₆- b -PDL- b -Glc₆, it is quite reasonable to consider that Glc₄-(PDL- b -Glc₄)₂ and (Glc₃)₂-(PDL- b -Glc₃)₂ formed the BCC structure. However, interestingly, the d_{s-s} values of Glc₄-(PDL- b -Glc₄)₂ and (Glc₃)₂-(PDL- b -Glc₃)₂ ($d_{s-s} = 10.3$ and 9.7 nm, respectively) were significantly smaller than that of Glc₆- b -PDL- b -Glc₆ ($d_{s-s} = 13.4$ nm). Such a tendency was also clearly observed by AFM imaging (Figures 4d and 4e). The d_{AFM} values for Glc₄-(PDL- b -Glc₄)₂ and (Glc₃)₂-(PDL- b -Glc₃)₂ were determined to be 8.7 and 8.2 nm, respectively, which are smaller than that of Glc₆- b -PDL- b -Glc₆ ($d_{AFM} = 11.9$ nm). This could be related to the fact that the PDL chain lengths between the two saccharide segments in Glc₄-(PDL- b -Glc₄)₂ and (Glc₃)₂-(PDL- b -Glc₃)₂ are shorter than that of Glc₆- b -PDL- b -Glc₆.

Finally, we examined the wide-angle X-ray scattering (WAXS) for the thermally-annealed specimens (Figure S17) to reveal the physical state, i.e., glassy or crystalline, of the oligosaccharide domain. Note that all the WAXS data were collected at the same time as the SAXS measurements. As shown in Figure S17, only a broad amorphous halo peak was observed for all the samples, demonstrating no crystallization. Considering the fact that the T_g of the oligosaccharide block are well above room temperature, it can be concluded that the oligosaccharide domains in all the specimens are in the glassy state.

Mechanical Properties

The thermally-annealed BCP films, which were the same samples used for the SAXS experiments, were cut into a dog-bone-shaped geometry and subjected to tensile testing to investigate their mechanical properties. All specimens were transparent, soft, flexible, and non-tacky. Given that PDL itself is a viscous liquid, the elastomeric properties of the BCPs can be attributed to the physical crosslinking of the rubbery PDL chains by the oligosaccharide hard segments. Figure 5 shows the typical stress-strain curves of the BCP specimens, and Table 2 summarizes the key mechanical properties, i.e., the Young's modulus (E), strain at break (ϵ_b), stress at break (σ_b), and toughness, along with the average values, standard deviations, and other key material characteristics. No BCP specimens exhibited any distinct yielding point, and showed elongation with only a small degree of stress, as would be expected for soft elastomers. At a low strain, a linear increase in the stress was observed for all specimens upon stretching, and the E value was estimated from the slope. Among the BCPs, (Glc₃)₂-*b*-PDL-*b*-(Glc₃)₂ exhibited the best mechanical performance with an E of 6.8 ± 1.1 MPa, an ϵ_b of $236 \pm 39.6\%$, a σ_b of 4.6 ± 0.69 MPa, and a toughness of 7.1 ± 2.0 MJ m⁻³. It is notable that the E value is comparable to that of well-known styrene-based thermoplastic elastomers (>6.0 MPa).⁴³ Interestingly, the E , σ_b , and toughness values of the HEX-forming BCPs (i.e., (Glc₃)₂-*b*-PDL-*b*-(Glc₃)₂ and (Glc₂)₃-*b*-PDL-*b*-(Glc₂)₃) were significantly higher than those of the BCC-forming BCPs (i.e., Glc₆-*b*-PDL-*b*-Glc₆, Glc₄-(PDL-*b*-Glc₄)₂, and (Glc₃)₂-(PDL-*b*-Glc₃)₂). Normally, an increase in the hard segment fraction results in an increase in the E value. However, the f_{sac} values of our BCPs were fixed at 0.11–0.13, and therefore, the distinct differences in the mechanical properties should stem from the microphase-separated morphology: the continuous hard domain in the HEX-forming BCPs can bear the deformation upon stretching, resulting in higher E values. Meanwhile, the hard sphere domains in the BCC-forming BCPs are isolated

from one another, so that only the rubbery PDL matrix bear the deformation upon stretching, resulting in lower E values. When comparing among the HEX-forming BCPs, $(\text{Glc}_3)_2$ -*b*-PDL-*b*- $(\text{Glc}_3)_2$ exhibited better ε_b value. As discussed before, the PDL chain in $(\text{Glc}_3)_2$ -*b*-PDL-*b*- $(\text{Glc}_3)_2$ is less stretched, due to the higher interfacial curvature, compared to $(\text{Glc}_2)_3$ -*b*-PDL-*b*- $(\text{Glc}_2)_3$. Thus, the PDL chain in $(\text{Glc}_3)_2$ -*b*-PDL-*b*- $(\text{Glc}_3)_2$ should have better capacity to elongate, which could contribute to the improved ε_b value.

Table 2. Tensile properties and the other key material characteristics of the carbohydrate-based elastomers^a

BCP	E^a (MPa)	ε_b^a (%)	σ_b^a (MPa)	toughness ^a (MJ m ⁻³)	morphology ^b	d^c (nm)	$T_{g,PDL}^d$ (°C)	$T_{g,sac}^d$ (°C)
Glc ₆ - <i>b</i> -PDL- <i>b</i> -Glc ₆	1.1 ± 0.066	86.2 ± 11.1	0.50 ± 0.065	0.28 ± 0.064	BCC	13.6	-50	143
(Glc ₃) ₂ - <i>b</i> -PDL- <i>b</i> -(Glc ₃) ₂	6.8 ± 1.1	236 ± 39.6	4.6 ± 0.69	7.1 ± 2.0	HEX	12.6	-49	115
(Glc ₂) ₃ - <i>b</i> -PDL- <i>b</i> -(Glc ₂) ₃	6.2 ± 1.3	102 ± 52.7	2.5 ± 0.93	1.9 ± 1.5	HEX	14.4	-49	85
Glc ₄ -(PDL- <i>b</i> -Glc ₄) ₂	2.6 ± 0.17	115 ± 5.7	1.6 ± 0.092	1.1 ± 0.096	BCC	10.3	-49	114
(Glc ₃) ₂ -(PDL- <i>b</i> -Glc ₃) ₂	2.4 ± 0.20	59.5 ± 3.9	0.90 ± 0.028	0.32 ± 0.024	BCC	9.7	-48	84

^aAll specimens were thermally annealed at 180 °C for 3 h. Tensile properties are shown as an average value (with standard deviation) for at least three specimens. ^bMorphology in the bulk state was determined by SAXS. ^cInterdomain distance (d) was calculated as $(2\pi/q^*) (3/2)^{1/2}$ for BCC and $(2\pi/q^*) (4/3)^{1/2}$ for HEX based on SAXS. ^dDetermined by DSC during the second heating run.

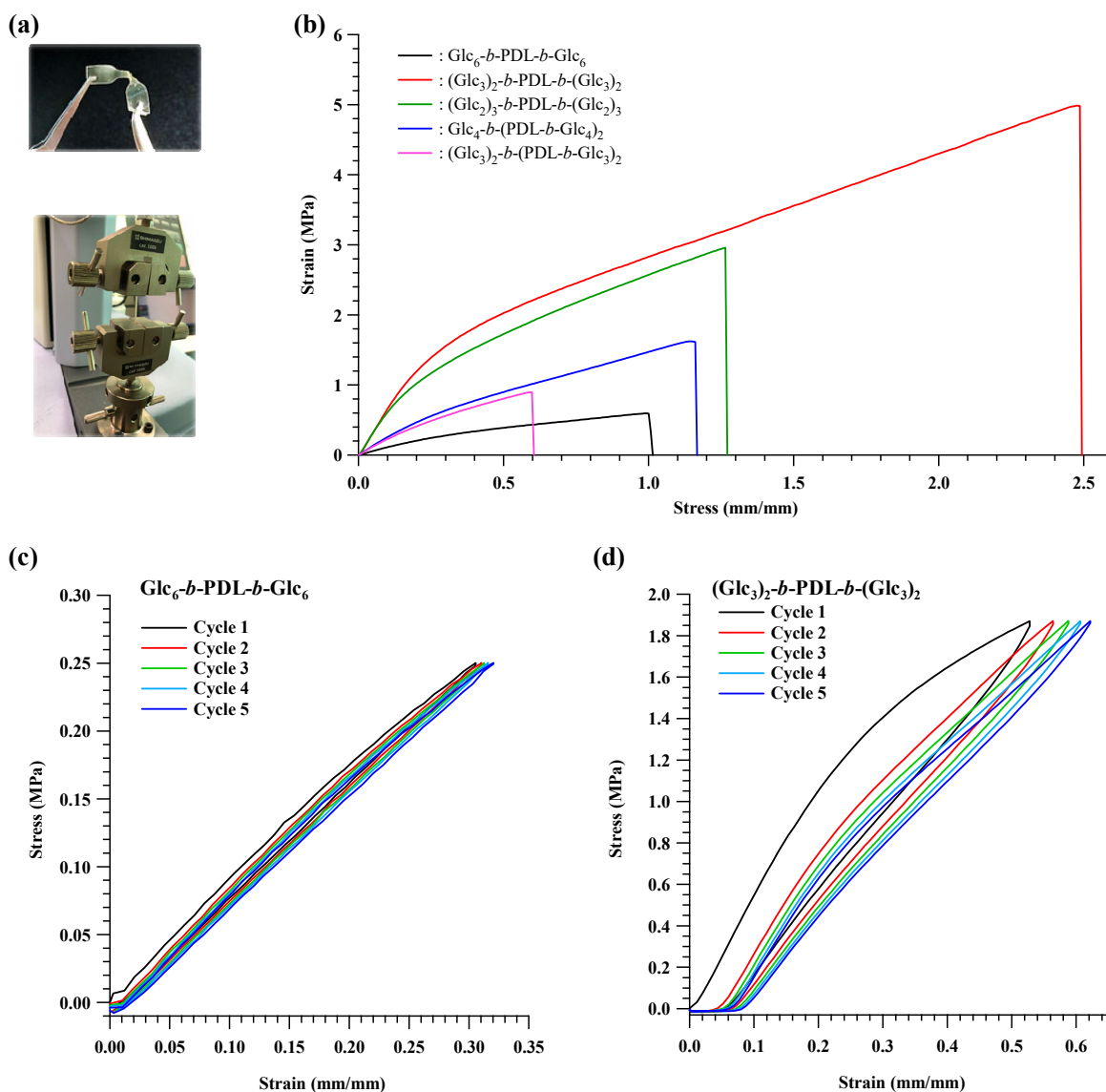


Figure 5. Tensile testing of the carbohydrate-based elastomers. (a) Photographic images of a typical specimen for the tensile test. (b) Typical stress-strain curves (crosshead speed, 10 mm min^{-1}) of the $\text{Glc}_6\text{-}b\text{-PDL-}b\text{-Glc}_6$, $(\text{Glc}_3)_2\text{-}b\text{-PDL-}b\text{-}(\text{Glc}_3)_2$, $(\text{Glc}_2)_3\text{-}b\text{-PDL-}b\text{-}(\text{Glc}_2)_3$, $\text{Glc}_4\text{-}(PDL\text{-}b\text{-Glc}_4)_2$, and $(\text{Glc}_3)_2\text{-}(PDL\text{-}b\text{-Glc}_3)_2$ specimens after thermal annealing ($180 \text{ }^\circ\text{C}$ for 3 h). (c and d) Cyclic tensile testing results (crosshead speed, 10 mm min^{-1}) for the $\text{Glc}_6\text{-}b\text{-PDL-}b\text{-Glc}_6$ and $(\text{Glc}_3)_2\text{-}b\text{-PDL-}b\text{-}(\text{Glc}_3)_2$ specimens after thermal annealing ($180 \text{ }^\circ\text{C}$ for 3 h).

Upon comparing the different BCC-forming BCPs, the E value of $\text{Glc}_6\text{-}b\text{-PDL-}b\text{-Glc}_6$ was found to be lower than those of $\text{Glc}_4\text{-}(PDL\text{-}b\text{-Glc}_4)_2$ and $(\text{Glc}_3)_2\text{-}(PDL\text{-}b\text{-Glc}_3)_2$, which was attributed to

the morphological differences. Considering the d value for the BCC morphology, the number density of the hard sphere domain in the $\text{Glc}_4\text{-(PDL-}b\text{-Glc}_4)_2$ and $(\text{Glc}_3)_2\text{-(PDL-}b\text{-Glc}_3)_2$ specimens is higher than that of $\text{Glc}_6\text{-}b\text{-PDL-}b\text{-Glc}_6$, despite these three BCPs possessing a comparable total molecular weight and f_{sac} value. The higher crosslinking density is therefore likely to be responsible for the enhanced E value. These results indicate that the mechanical properties of the carbohydrate-based elastomers are essentially determined by the microphase-separated morphology, but are not affected by the oligosaccharide chain length.

Subsequently, we performed a cyclic tensile test on the BCP specimens to understand the elastic recovery and level of plastic deformation. Here, $\text{Glc}_6\text{-}b\text{-PDL-}b\text{-Glc}_6$ and $(\text{Glc}_3)_2\text{-}b\text{-PDL-}b\text{-(Glc}_3)_2$ were taken as representative examples of BCC- and HEX-forming BCPs. Each dog-bone-shaped specimen was subjected to five loading/unloading cycles at a strain of 30% for $\text{Glc}_6\text{-}b\text{-PDL-}b\text{-Glc}_6$ and 50% for $(\text{Glc}_3)_2\text{-}b\text{-PDL-}b\text{-(Glc}_3)_2$, with a constant crosshead speed (10 mm min^{-1}). The $\text{Glc}_6\text{-}b\text{-PDL-}b\text{-Glc}_6$ specimen exhibited a small hysteresis loop with a negligible residual strain (ca. 1%). As discussed above, the hard sphere domains are isolated in this BCP, and so no obvious plastic deformation was observed at this strain level. In contrast, the $(\text{Glc}_3)_2\text{-}b\text{-PDL-}b\text{-(Glc}_3)_2$ specimen exhibited a larger hysteresis loop in the first cycle, likely due to the initial alignment of the hard cylinder domain. Nevertheless, the residual strain for this specimen was ca. 7%, even after the five loading/unloading cycles with a maximum strain of 50%. These results confirmed the sufficient level of elastic recovery of the carbohydrate-based elastomers.

BCPs from Readily Available Maltooligosaccharides

In the above investigations, the clear correlation between the molecular structure and the physical properties was successfully discussed based on the monodisperse maltooligosaccharides with a defined degree of polymerization (DP) as the hard segment. However, the critical drawback of using such monodisperse oligosaccharides is their limited availability, with the majority being rather expensive. Thus, we turned our attention to the polydisperse maltooligosaccharides which are inexpensive, readily available from the food industry, and widely used as food additives. Starting from a commercially available maltooligosaccharide syrup (Fujioligo G67 from NIHON SHOKUJIN KAKO CO., LTD., Tokyo, Japan), we prepared an ethynyl-functionalized maltooligosaccharide with an average DP of 5.8 (i.e., $\text{Glc}_6^*-\text{C}\equiv\text{CH}$) and a D value of 1.11 by following the same protocol as that employed for the synthesis of $\text{Glc}_6-\text{C}\equiv\text{CH}$ (see section S5 in the SI for details). The previous investigations revealed that the mechanical properties of the A_2BA_2 type BCP is superior to those of the ABA counterpart. Therefore, $\text{Glc}_6^*-\text{C}\equiv\text{CH}$ was subjected to click-reaction with $(\text{N}_3)_2\text{-PDL}_{20\text{k}}\text{-(N}_3)_2$ ($M_{\text{n,NMR}} = 18700 \text{ g mol}^{-1}$, $D = 1.11$) to produce the A_2BA_2 -type BCP with a higher molecular weight, i.e., $(\text{Glc}_6^*)_2\text{-}b\text{-PDL}_{20\text{k}}\text{-}b\text{-(Glc}_6^*)_2$ ($M_{\text{n}} = 27200 \text{ g mol}^{-1}$, $D = 1.18$). It should be noted here that the volume fraction of $(\text{Glc}_6^*)_2\text{-}b\text{-PDL}_{20\text{k}}\text{-}b\text{-(Glc}_6^*)_2$ was designed to be comparable to that of $(\text{Glc}_3)_2\text{-}b\text{-PDL}\text{-}b\text{-(Glc}_3)_2$. For comparison purposes, the linear counterpart, i.e., $\text{Glc}_6^*\text{-}b\text{-PDL}_{12\text{k}}\text{-}b\text{-Glc}_6^*$ ($M_{\text{n}} = 12400 \text{ g mol}^{-1}$, $D = 1.11$), was also prepared starting from $\text{N}_3\text{-PDL}_{12\text{k}}\text{-N}_3$ ($M_{\text{n}} = 8400 \text{ g mol}^{-1}$, $D = 1.13$).

SAXS analysis of the thermally-annealed solvent cast films revealed that $\text{Glc}_6^*\text{-}b\text{-PDL}_{10\text{k}}\text{-}b\text{-Glc}_6^*$ and $(\text{Glc}_6^*)_2\text{-}b\text{-PDL}_{20\text{k}}\text{-}b\text{-(Glc}_6^*)_2$ formed the BCC ($d_{\text{s-s}} = 12.4 \text{ nm}$) and HEX ($d_{\text{c-c}} = 17.8 \text{ nm}$) structures with high degree of ordering, respectively, despite the significant increase in the D

value of the oligosaccharide segment (Figures 6a and 6b). The AFM images of the thermally-annealed thin films also supported the SAXS results (Figures 6c and 6d). No obvious differences in the tensile properties were observed for the $\text{Glc}_6^*-b\text{-PDL}_{10k}\text{-}b\text{-Glc}_6^*$ samples when compared with the monodisperse $\text{Glc}_6\text{-}b\text{-PDL}_{10k}\text{-}b\text{-Glc}_6$ counterpart (Figure 6e). However, surprisingly, dramatic improvements in the ε_b , σ_b , and toughness values were observed for $(\text{Glc}_6^*)_2\text{-}b\text{-PDL}_{20k}\text{-}b\text{-}(\text{Glc}_6^*)_2$ compared with $(\text{Glc}_3)_2\text{-}b\text{-PDL}\text{-}b\text{-}(\text{Glc}_3)_2$, despite both BCPs possessing a comparable f_{sac} . Importantly, the ε_b value of the $(\text{Glc}_6^*)_2\text{-}b\text{-PDL}_{20k}\text{-}b\text{-}(\text{Glc}_6^*)_2$ specimen reached $658 \pm 87\%$, which is approximately three times that of $(\text{Glc}_3)_2\text{-}b\text{-PDL}\text{-}b\text{-}(\text{Glc}_3)_2$. The enhanced tensile properties therefore likely stem from the enhanced chain entanglement of the rubbery PDL block. It is well known that the mechanical properties of thermoplastic elastomers are highly dependent on the entanglement molecular weight (M_e).^{44,45} For $(\text{Glc}_3)_2\text{-}b\text{-PDL}\text{-}b\text{-}(\text{Glc}_3)_2$, the M_n of the middle PDL block is lower than the reported M_e value of PDL (13.5 kg mol^{-1}),³³ which means that the PDL chains are unentangled, thereby resulting in insufficient tensile properties. Meanwhile, the PDL chain length of $(\text{Glc}_6^*)_2\text{-}b\text{-PDL}_{20k}\text{-}b\text{-}(\text{Glc}_6^*)_2$ is higher than the M_e , which should account for the considerable enhancement in the ε_b , σ_b , and toughness values. In contrast, no significant differences were found in the E values between $(\text{Glc}_3)_2\text{-}b\text{-PDL}\text{-}b\text{-}(\text{Glc}_3)_2$ and $(\text{Glc}_6^*)_2\text{-}b\text{-PDL}_{20k}\text{-}b\text{-}(\text{Glc}_6^*)_2$, again suggesting that the dominant factor in terms of determining the E value is the microphase-separated morphology, i.e., the HEX structure, but not the length of each oligosaccharide segment.

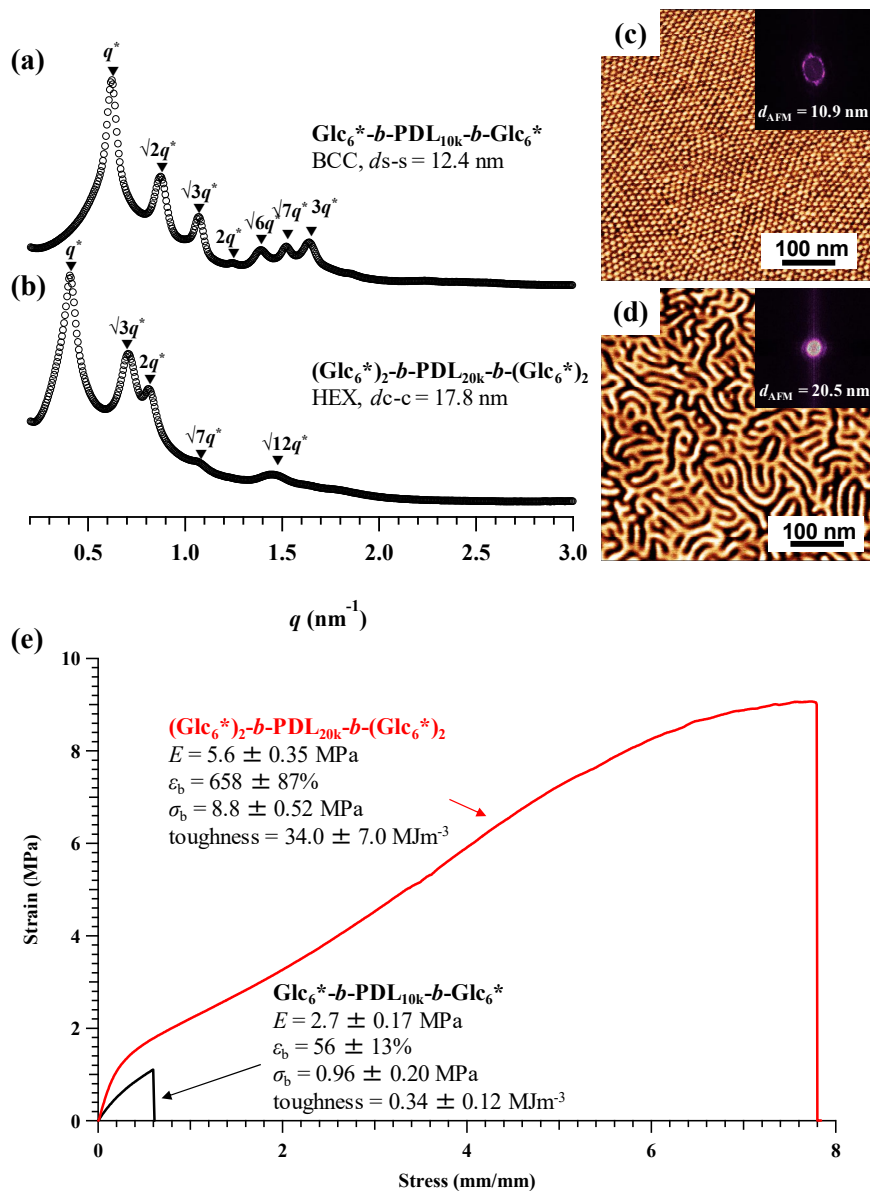


Figure 6. Morphological characterization and tensile properties of the BCPs prepared using the polydisperse maltooligosaccharide. (a and b) SAXS profiles of $\text{Glc}_6^* \text{-} b \text{-PDL}_{10\text{k}} \text{-} b \text{-Glc}_6^*$ and $(\text{Glc}_6^*)_2 \text{-} b \text{-PDL}_{20\text{k}} \text{-} b \text{-}(\text{Glc}_6^*)_2$ after thermal annealing at $180 \text{ }^\circ\text{C}$ for 3 h. (c and d) AFM phase images of $\text{Glc}_6^* \text{-} b \text{-PDL}_{10\text{k}} \text{-} b \text{-Glc}_6^*$ and $(\text{Glc}_6^*)_2 \text{-} b \text{-PDL}_{20\text{k}} \text{-} b \text{-}(\text{Glc}_6^*)_2$ thin films after thermal annealing at $180 \text{ }^\circ\text{C}$ for 3 h. (e) Typical stress-strain curve of $\text{Glc}_6^* \text{-} b \text{-PDL}_{10\text{k}} \text{-} b \text{-Glc}_6^*$ and $(\text{Glc}_6^*)_2 \text{-} b \text{-PDL}_{20\text{k}} \text{-} b \text{-}(\text{Glc}_6^*)_2$ after thermal annealing at $180 \text{ }^\circ\text{C}$ for 3 h.

Conclusions

In summary, we successfully synthesized “hard-*b*-soft-*b*-hard” type triblock copolymers consisting of maltooligosaccharide as the hard segment and poly(δ -decanolactone) (PDL) as the soft segment. This was achieved using naturally occurring raw materials, and the obtained copolymers were found to behave as elastomers, in which the microphase-separated oligosaccharide domain acts as the physical crosslinker between the rubbery PDL chains. Importantly, it was found that the mechanical properties of the carbohydrate-based elastomers were mainly determined by the microphase-separated structure (morphology and domain-spacing) and were less affected by the length of each oligosaccharide chain. In contrast, the T_g of the hard segment was indeed affected by the oligosaccharide chain length. Remarkably, some of the carbohydrate-based elastomers exhibited a Young modulus comparable to conventional styrene-based thermoplastic elastomers, and a stress at break of approximately 700% was achieved when combining the higher molecular weight PDL and readily available polydisperse maltooligosaccharides. Our results therefore demonstrate that oligo/polysaccharides can be considered a sustainable alternative to petroleum-derived synthetic hard segments, which could therefore open a new avenue to bio-based soft materials. The maltooligosaccharides (or amylose) are edible and therefore not best suited to future applications. Instead, other non-edible oligo/polysaccharides, e.g., cellulose, chitin, chitosan, dextran, and their derivatives, could be applied to the bio-based elastomer design. Considering the bio-based and sustainable nature of our system, in addition to the biodegradability and biocompatibility of carbohydrate-based elastomers, these structures could be considered attractive as next-generation bio-based polymeric materials for application in sanitary, cosmetic, environmental, and medical uses, as well as for the soft substrates of wearable electronic devices.

ASSOCIATED CONTENT

Supporting Information.

The Supporting Information is available free of charge via the Internet at <http://pubs.acs.org>.

Experimental details, ¹H NMR, IR, TGA, DSC, SEC, and MALDI-TOF MS data.

AUTHOR INFORMATION

Corresponding Author

*Takuya Isono; Email: isono.t@eng.hokudai.ac.jp

*Toshifumi Satoh; Email: satoh@eng.hokudai.ac.jp

Funding Sources

This work was financially supported by a JSPS Grant-in-Aid for Scientific Research (B) (No. 19H02769, T.S.), a JSPS Grant-in-Aid for Young Scientists (No. 18K14268, T.I.), the Photo-excitonix Project (Hokkaido University, T.S.), the Frontier Chemistry Center (Hokkaido University, T.I.), the Iketani Science and Technology Foundation (T.I.), the Asahi Glass Foundation (T.I.), and Toyota Riken (T.I.).

ACKNOWLEDGMENT

This work was, in part, performed under the approval of the Photon Factory Program Advisory Committee (Proposal No. 2017G589 and 2019G579). T.I. gratefully acknowledges the Nanotech CUPAL NRP program. We thank Prof. Hajime Ito and Prof. Ken-ichiro Matsumoto (Hokkaido University) for their assistance with the AFM experiments and tensile testing, respectively. We thank NIHON SHOKUJIN KAKO CO., LTD. for kindly providing Fujioligo G67.

REFERENCES

- (1) Climent, M. J.; Corma, A.; Iborra, S. Converting carbohydrates to bulk chemicals and fine chemicals over heterogeneous catalysts. *Green Chem.* **2011**, *13*, 520-540.
- (2) Lichtenthaler, F. W.; Peters, S. Carbohydrates as green raw materials for the chemical industry. *C. R. Chimie* **2004**, *7*, 65-90.
- (3) Esposito, D.; Antonietti, M. Redefining biorefinery: the search for unconventional building blocks for materials. *Chem. Soc. Rev.* **2015**, *44*, 5821-5835.
- (4) Bozell, J. J.; Petersen, G. R. Technology development for the production of biobased products from biorefinery carbohydrates—the US Department of Energy’s “Top 10” revisited. *Green Chem.* **2010**, *12*, 539-554.
- (5) Zhu, Y.; Romain, C.; Williams, C. K. Sustainable polymers from renewable resources. *Nature* **2016**, *540*, 354-362.
- (6) Gregory, G. L.; López-Vidal, E. M.; Buchard, A. Polymers from sugars: cyclic monomer synthesis, ring-opening polymerisation, material properties and applications. *Chem. Commun.* **2017**, *53*, 2198-2217.

- (7) Gandini, A.; Lacerda, T. M. From monomers to polymers from renewable resources: Recent advances. *Prog. Polym. Sci.* **2015**, *48*, 1-39.
- (8) Gandini, A. Polymers from Renewable Resources: A Challenge for the Future of Macromolecular Materials. *Macromolecules* **2008**, *41*, 9491-9504.
- (9) Muñoz-Guerra, S.; Lavilla, C.; Japu, C.; de Ilarduya, A. M. Renewable terephthalate polyesters from carbohydrate-based bicyclic monomers. *Green Chem.* **2014**, *16*, 1716-1739.
- (10) Adhikari, R.; Hichler, G. H. Influence of molecular architecture on morphology and micromechanical behavior of styrene/butadiene block copolymer systems. *Prog. Polym. Sci.* **2004**, *29*, 949-986.
- (11) Wang, W.; Lu, W.; Goodwin, A.; Wang, H.; Yin, P.; Kang, N.-G.; Hong, K.; Mays, J. W. Recent advances in thermoplastic elastomers from living polymerizations: Macromolecular architectures and supramolecular chemistry *Prog. Polym. Sci.* **2019**, *95*, 1-31.
- (12) Otsuka, I.; Isono, T.; Rochas, C.; Halila, S.; Fort, S.; Satoh, T.; Kakuchi, T.; Borsali, R. 10 nm Scale Cylinder–Cubic Phase Transition Induced by Caramelization in Sugar-Based Block Copolymers. *ACS Macro Lett.* **2012**, *1*, 1379-1382.
- (13) Isono, T.; Otsuka, I.; Kondo, Y.; Halila, S.; Fort, S.; Rochas, C.; Satoh, T.; Borsali, R.; Kakuchi, T. Sub-10 nm Nano-Organization in AB₂- and AB₃-Type Miktoarm Star Copolymers Consisting of Maltoheptaose and Polycaprolactone *Macromolecules* **2013**, *46*, 1461-1469.
- (14) Isono, T.; Otsuka, I.; Suemasa, D.; Rochas, C.; Satoh, T.; Borsali, R.; Kakuchi, T. Synthesis, Self-Assembly, and Thermal Caramelization of Maltoheptaose-Conjugated Polycaprolactones Leading to Spherical, Cylindrical, and Lamellar Morphologies. *Macromolecules* **2013**, *46*, 8932-8940.

- (15) Otsuka, I.; Zhang, Y.; Isono, T.; Rochas, C.; Kakuchi, T.; Satoh, T.; Borsali, R. Sub-10 nm Scale Nanostructures in Self-Organized Linear Di- and Triblock Copolymers and Miktoarm Star Copolymers Consisting of Maltoheptaose and Polystyrene. *Macromolecules* **2015**, *48*, 1509-1517.
- (16) Yoshida, K.; Tanaka, S.; Yamamoto, T.; Tajima, K.; Borsali, R.; Isono, T.; Satoh, T. Chain-End Functionalization with a Saccharide for 10 nm Microphase Separation: “Classical” PS-*b*-PMMA versus PS-*b*-PMMA-Saccharide *Macromolecules* **2018**, *51*, 8870-8877.
- (17) Hung, C.-C.; Nakahira, S.; Chiu, Y.-C.; Isono, T.; Wu, H.-C.; Watanabe, K.; Chiang, Y.-C.; Takashima, S.; Borsali, R.; Tung, S.-H.; Satoh, T.; Chen, W.-C. Control over Molecular Architectures of Carbohydrate-Based Block Copolymers for Stretchable Electrical Memory Devices. *Macromolecules* **2018**, *51*, 4966-4975.
- (18) Isono, T.; Ree, B. J.; Tajima, K.; Borsali, R.; Satoh, T. Highly Ordered Cylinder Morphologies with 10 nm Scale Periodicity in Biomass-Based Block Copolymers. *Macromolecules* **2018**, *51*, 428-437.
- (19) Isono, T.; Kawakami, N.; Watanabe, K.; Yoshida, K.; Otsuka, I.; Mamiya, H.; Ito, H.; Yamamoto, T.; Tajima, K.; Borsali, R.; Satoh, T. Microphase separation of carbohydrate-based star-block copolymers with sub-10 nm periodicity. *Polym. Chem.* **2019**, *10*, 1119-1129.
- (20) Thomas, T. S.; Hwang, W.; Sita, L. R. End-Group-Functionalized Poly(α -olefinates) as Non-Polar Building Blocks: Self-Assembly of Sugar-Polyolefin Hybrid Conjugates. *Angew. Chem. Int. Ed.* **2016**, *55*, 4683-4687.

- (21) Nowak, S. R.; Hwang, W.; Sita, L. R. Dynamic Sub-10-nm Nanostructured Ultrathin Films of Sugar-Polyolefin Conjugates Thermoresponsive at Physiological Temperatures. *J. Am. Chem. Soc.* **2017**, *139*, 5281-5284.
- (22) Lachmayer, K. K.; Wentz, C. M.; Sita, L. R. An Exceptionally Stable and Scalable Sugar-Polyolefin Frank-Kasper A15 Phase. *Angew. Chem. Int. Ed.* **2020**, *59*, 1521-1526.
- (23) Lachmayer, K. K.; Sita, L. R. Small-Molecule Modulation of Soft Matter Frank-Kasper Phases: A Method for Adding Function to Form. *Angew. Chem. Int. Ed.* **2020**, *59*, 3563-3595.
- (24) Martello, M. T.; Burns, A.; Hillmyer, M. A. Bulk Ring-Opening Transesterification Polymerization of the Renewable δ -Decalactone Using an Organocatalyst. *ACS Macro Lett.* **2012**, *1*, 131-135.
- (25) Rali, T.; Wossa, S.W.; Leach, D. N. Comparative Chemical Analysis of the Essential Oil Constituents in the Bark, Heartwood and Fruits of *Cryptocarya massoy* (Oken) Kosterm. (Lauraceae) from Papua New Guinea. *Molecules* **2007**, *12*, 149-154.
- (26) Honeker, C. C.; Thomas, E. L. Impact of Morphological Orientation in Determining Mechanical Properties in Triblock Copolymer Systems. *Chem. Mater.* **1996**, *8*, 1702-1714.
- (27) Dair, B. J.; Honeker, C. C.; Alward, D. B.; Avgeropoulos, A.; Hadjichristidis, N.; Fetters, L. J.; Capel, M.; Thomas, E. L. Mechanical Properties and Deformation Behavior of the Double Gyroid Phase in Unoriented Thermoplastic Elastomers. *Macromolecules* **1999**, *32*, 8145-8152.
- (28) Shin, J.; Martello, M. T.; Shrestha, M.; Wissinger, J. E.; Tolman, W. B.; Hillmyer, M. A. Pressure-Sensitive Adhesives from Renewable Triblock Copolymers. *Macromolecules* **2011**, *44*, 87-94.

- (29) Zhou, C.; Wei, Z.; Lei, X.; Li, Y. Fully biobased thermoplastic elastomers: synthesis and characterization of poly(L-lactide)-*b*-polymyrcene-*b*-poly(L-lactide) triblock copolymers. *RSC Adv.* **2016**, *6*, 63508-63514.
- (30) Huang, Y.; Chang, R.; Han, L.; Shan, G.; Bao, Y.; Pan, P. ABA-Type Thermoplastic Elastomers Composed of Poly(ϵ -caprolactone-*co*- δ -valerolactone) Soft Midblock and Polymorphic Poly(lactic acid) Hard End blocks. *ACS Sustainable Chem. Eng.* **2016**, *4*, 121-128.
- (31) C. L. Wanamaker, M. J. Bluemle, L. M. Pitet, L. E. O’Leary, W. B. Tolman and, M. A. Hillmyer, *Biomacromolecules*, 2009, **10**, 2904.
- (32) Lee, S.; Yuk, J. S.; Park, H.; Kim, Y.-K.; Shin, J. Multiblock Thermoplastic Elastomers Derived from Biodiesel, Poly(propylene glycol), and L-Lactide. *ACS Sustainable Chem. Eng.* **2017**, *5*, 8148-8160.
- (33) Shin, J.; Lee, Y.; Tolman, W. B.; Hillmyer, M. A. Thermoplastic Elastomers Derived from Menthide and Tulipalin A. *Biomacromolecules* **2012**, *13*, 3833-3840.
- (34) Ganewatta, M. S.; Ding, W.; Rahman, M. A.; Yuan, L.; Wang, Z.; Hamidi, N.; Robertson, M. L.; Tang, C. Biobased Plastics and Elastomers from Renewable Rosin via “Living” Ring-Opening Metathesis Polymerization *Macromolecules* **2016**, *49*, 7155-7164.
- (35) Satoh, K.; Lee, D.-H.; Nagai, K.; Kamigaito, M. Precision Synthesis of Bio-Based Acrylic Thermoplastic Elastomer by RAFT Polymerization of Itaconic Acid Derivatives. *Macromol. Rapid Commun.* **2014**, *35*, 161-167.
- (36) Saito, T.; Aizawa, Y.; Tajima, K.; Isono, T.; Satoh, T. Organophosphate-catalyzed bulk ring-opening polymerization as an environmentally benign route leading to block copolyesters,

- end-functionalized polyesters, and polyester-based polyurethane. *Polym. Chem.* **2015**, *6*, 4374-4384.
- (37)Schneiderman, D. K.; Hillmyer, M. A. Aliphatic Polyester Block Polymer Design. *Macromolecules* **2016**, *49*, 2419-2428.
- (38)Isono, T.; Kamoshida, K.; Satoh, Y.; Takaoka, T.; Sato, S.-i.; Satoh, T.; Kakuchi, T. Synthesis of Star- and Figure-Eight-Shaped Polyethers by *t*-Bu-P₄-Catalyzed Ring-Opening Polymerization of Butylene Oxide. *Macromolecules* **2013**, *46*, 3841–3849.
- (39)Imamura, K.; Sakaura, K.; Ohyama, K.-i.; Fukushima, A.; Imanaka, H.; Sakiyama, T.; Nakanishi, K. Temperature Scanning FTIR Analysis of Hydrogen Bonding States of Various Saccharides in Amorphous Matrixes below and above Their Glass Transition Temperatures. *J. Phys. Chem. B* **2006**, *110*, 15094-15099.
- (40)Hadjichristidis, N.; Iatrou, H.; Behal, S. K.; Chludzinski, J. J.; Disko, M. M.; Garner, R. T.; Liang, K. S.; Lohse, D. J.; Milner, S. T. Morphology and miscibility of miktoarm styrene-diene copolymers and terpolymers. *Macromolecules* **1993**, *26*, 5812-5815.
- (41)Milner, S. T. Chain Architecture and Asymmetry in Copolymer Microphases. *Macromolecules* **1994**, *27*, 2333-2335.
- (42)Pochan, D. J.; Gido, S. P.; Pispas, S.; Mays, J. W.; Ryan, A. J.; Fairclough, J. P. A.; Hamley, I. W.; Terrill, N. J. *Macromolecules* **1996**, *29*, 5091-5098.
- (43)Holden, G.; Legge, N. R.; Quirk, R. P.; Schroeder, H. E. *Thermoplastic Elastomers*, 2nd ed. Hanser Gardner Pubns, **1996**.
- (44)Drobny, J. G. *Handbook of Thermoplastic Elastomers*, 2nd ed. William Andrew, **2014**.

(45) Fetters, L. J.; Lohse, D. J.; Milner, S. T.; Graessley, W. W. Packing Length Influence in Linear Polymer Melts on the Entanglement, Critical, and Reputation Molecular Weights. *Macromolecules* **1999**, *32*, 6847-6851.